CLEO CONF 96-05
ICHEP96 PA05-093

Radiative Penguin Decays of the B Meson

CLEO Collaboration

(July 23, 1996)

Abstract

With 2.6×10^6 $B\bar{B}$ pairs taken with the CLEO II detector at CESR, we study the electromagnetic penguin decays $B \to K^*(892)\gamma$. Using a maximum likelihood fit we measure $Br(B \to K^*\gamma) = (4.2 \pm 0.8 \pm 0.6) \times 10^{-5}$ from the following decay channels: $B^0 \to K^{*0}\gamma$, ($K^{*0} \to K^+\pi^-$ and $K^0\pi^0$) and $B^- \to K^{*-}\gamma$, ($K^{*-} \to K^0\pi^-$ and $K^-\pi^0$). Combining our new measurement with the recent inclusive rate we find $\Gamma(B \to K^*\gamma)/\Gamma(b \to s\gamma) = 0.181 \pm 0.068$. In addition we have searched for exclusive $b \to d\gamma$ decays and placed upper limits on $Br(B^0 \to \rho^0\gamma) < 3.9 \times 10^{-5}$, $Br(B^0 \to \omega\gamma) < 1.3 \times 10^{-5}$, and $Br(B^- \to \rho^-\gamma) < 1.1 \times 10^{-5}$. Combining these measurements with our new measurement of $Br(B \to K^*\gamma)$ we place a limit on $|V_{td}/V_{ts}| < 0.45 - 0.56$.

R. Ammar,[1] P. Baringer,[1] A. Bean,[1] D. Besson,[1] D. Coppage,[1] C. Darling,[1] R. Davis,[1] N. Hancock,[1] S. Kotov,[1] I. Kravchenko,[1] N. Kwak,[1] S. Anderson,[2] Y. Kubota,[2] M. Lattery,[2] J. J. O'Neill,[2] S. Patton,[2] R. Poling,[2] T. Riehle,[2] A. Smith,[2] V. Savinov,[2] M. S. Alam,[3] S. B. Athar,[3] Z. Ling,[3] A. H. Mahmood,[3] H. Severini,[3] S. Timm,[3] F. Wappler,[3] A. Anastassov,[4] S. Blinov,[4,*] J. E. Duboscq,[4] R. Fulton,[4] D. Fujino,[4] K. K. Gan,[4] T. Hart,[4] K. Honscheid,[4] H. Kagan,[4] R. Kass,[4] J. Lee,[4] M. Sung,[4] A. Undrus,[4,*] R. Wanke,[4] A. Wolf,[4] M. M. Zoeller,[4] B. Nemati,[5] S. J. Richichi,[5] W. R. Ross,[5] P. Skubic,[5] M. Wood,[5] M. Bishai,[6] J. Fast,[6] E. Gerndt,[6] J. W. Hinson,[6] D. H. Miller,[6] E. I. Shibata,[6] I. P. J. Shipsey,[6] M. Yurko,[6] L. Gibbons,[7] S. D. Johnson,[7] Y. Kwon,[7] S. Roberts,[7] E. H. Thorndike,[7] C. P. Jessop,[8] K. Lingel,[8] H. Marsiske,[8] M. L. Perl,[8] S. F. Schaffner,[8] D. Ugolini,[8] R. Wang,[8] X. Zhou,[8] T. E. Coan,[9] V. Fadeyev,[9] I. Korolkov,[9] Y. Maravin,[9] I. Narsky,[9] V. Shelkov,[9] R. Stroynowski,[9] J. Staeck,[9] I. Volobouev,[9] J. Ye,[9] M. Artuso,[10] A. Efimov,[10] M. Gao,[10] M. Goldberg,[10] R. Greene,[10] F. Frasconi,[10] D. He,[10] S. Kopp,[10] G. C. Moneti,[10] R. Mountain,[10] Y. Mukhin,[10] S. Schuh,[10] T. Skwarnicki,[10] S. Stone,[10] X. Xing,[10] J. Bartelt,[11] S. E. Csorna,[11] V. Jain,[11] S. Marka,[11] A. Freyberger,[12] R. Godang,[12] D. Gibaut,[12] K. Kinoshita,[12] I. C. Lai,[12] P. Pomianowski,[12] S. Schrenk,[12] G. Bonvicini,[13] D. Cinabro,[13] L. Perera,[13] B. Barish,[14] M. Chadha,[14] S. Chan,[14] G. Eigen,[14] J. S. Miller,[14] C. O'Grady,[14] M. Schmidtler,[14] J. Urheim,[14] A. J. Weinstein,[14] F. Würthwein,[14] D. M. Asner,[15] D. W. Bliss,[15] W. S. Brower,[15] G. Masek,[15] H. P. Paar,[15] J. Gronberg,[16] C. M. Korte,[16] D. J. Lange,[16] R. Kutschke,[16] S. Menary,[16] R. J. Morrison,[16] S. Nakanishi,[16] H. N. Nelson,[16] T. K. Nelson,[16] C. Qiao,[16] J. D. Richman,[16] D. Roberts,[16] A. Ryd,[16] H. Tajima,[16] M. S. Witherell,[16] R. Balest,[17] B. H. Behrens,[17] K. Cho,[17] W. T. Ford,[17] H. Park,[17] P. Rankin,[17] J. Roy,[17] J. G. Smith,[17] J. P. Alexander,[18] C. Bebek,[18] B. E. Berger,[18] K. Berkelman,[18] K. Bloom,[18] D. G. Cassel,[18] H. A. Cho,[18] D. M. Coffman,[18] D. S. Crowcroft,[18] M. Dickson,[18] P. S. Drell,[18] R. Ehrlich,[18] R. Elia,[18] A. D. Foland,[18] P. Gaidarev,[18] B. Gittelman,[18] S. W. Gray,[18] D. L. Hartill,[18] B. K. Heltsley,[18] P. I. Hopman,[18] S. L. Jones,[18] J. Kandaswamy,[18] N. Katayama,[18] P. C. Kim,[18] D. L. Kreinick,[18] T. Lee,[18] Y. Liu,[18] G. S. Ludwig,[18] J. Masui,[18] J. Mevissen,[18] N. B. Mistry,[18] C. R. Ng,[18] E. Nordberg,[18] M. Ogg,[18,†] J. R. Patterson,[18] D. Peterson,[18] D. Riley,[18] A. Soffer,[18] C. Ward,[18] P. Avery,[19] M. Athanas,[19] C. D. Jones,[19] M. Lohner,[19] C. Prescott,[19] S. Yang,[19] J. Yelton,[19] J. Zheng,[19] G. Brandenburg,[20] R. A. Briere,[20] D. Y.-J. Kim,[20] T. Liu,[20] M. Saulnier,[20] R. Wilson,[20] H. Yamamoto,[20] T. E. Browder,[21] F. Li,[21] Y. Li,[21] J. L. Rodriguez,[21] T. Bergfeld,[22] B. I. Eisenstein,[22] J. Ernst,[22] G. E. Gladding,[22] G. D. Gollin,[22] E. Johnson,[22] I. Karliner,[22] M. Palmer,[22] M. Selen,[22] J. J. Thaler,[22] K. W. Edwards,[23] A. Bellerive,[24] D. I. Britton,[24] R. Janicek,[24] D. B. MacFarlane,[24] K. W. McLean,[24] P. M. Patel,[24] and A. J. Sadoff[25]

[1]University of Kansas, Lawrence, Kansas 66045
[2]University of Minnesota, Minneapolis, Minnesota 55455
[3]State University of New York at Albany, Albany, New York 12222

---

[*]Permanent address: BINP, RU-630090 Novosibirsk, Russia.

[†]Permanent address: University of Texas at Austin.

[4]Ohio State University, Columbus, Ohio 43210
[5]University of Oklahoma, Norman, Oklahoma 73019
[6]Purdue University, West Lafayette, Indiana 47907
[7]University of Rochester, Rochester, New York 14627
[8]Stanford Linear Accelerator Center, Stanford University, Stanford, California 94309
[9]Southern Methodist University, Dallas, Texas 75275
[10]Syracuse University, Syracuse, New York 13244
[11]Vanderbilt University, Nashville, Tennessee 37235
[12]Virginia Polytechnic Institute and State University, Blacksburg, Virginia 24061
[13]Wayne State University, Detroit, Michigan 48202
[14]California Institute of Technology, Pasadena, California 91125
[15]University of California, San Diego, La Jolla, California 92093
[16]University of California, Santa Barbara, California 93106
[17]University of Colorado, Boulder, Colorado 80309-0390
[18]Cornell University, Ithaca, New York 14853
[19]University of Florida, Gainesville, Florida 32611
[20]Harvard University, Cambridge, Massachusetts 02138
[21]University of Hawaii at Manoa, Honolulu, Hawaii 96822
[22]University of Illinois, Champaign-Urbana, Illinois 61801
[23]Carleton University, Ottawa, Ontario, Canada K1S 5B6
and the Institute of Particle Physics, Canada
[24]McGill University, Montréal, Québec, Canada H3A 2T8
and the Institute of Particle Physics, Canada
[25]Ithaca College, Ithaca, New York 14850

I. INTRODUCTION

The 1993 CLEO measurement of $B \to K^*\gamma$ [1] was the first direct evidence for penguin loop diagram decays. Precision measurement of the branching ratio of this decay mode can shed light on many fundamental issues in the Standard Model. It can be used to test non-perturbative QCD calculations, reduce theoretical uncertainty in the extraction of $|V_{ub}|$ from $B \to \rho l \nu$, and set limits on $|V_{td}/V_{ts}|$.

To calculate the $\Gamma(B \to K^*\gamma)/\Gamma(b \to s\gamma)$ ratio theorists must take into account non-perturbative QCD effects. With reduced statistical error, $\Gamma(B \to K^*\gamma)/\Gamma(b \to s\gamma)$ can be used as a test of different calculational methods at the two-loop level [2].

Measurements of $B \to K^*\gamma$ can be used to constrain the models used to calculate the form factors in $B \to \rho l \nu$ and thereby reduce the theoretical uncertainty in the extraction of $|V_{ub}|$. The decay $B \to \rho l \nu$ is of interest because its branching fraction is proportional to the CKM matrix element $|V_{ub}|$. Unfortunately, extracting $|V_{ub}|$ from the decay $B \to \rho l \nu$ is not trivial because the form factors governing the decay must be determined from non-perturbative QCD calculations. Isgur and Wise [3] have shown that in the limit of an infinite b quark mass (i.e. a static b quark), the semi-leptonic form factors are related to the $B \to \rho\gamma$ (or $\omega\gamma$) form factor near $q^2_{max} = (M_B - M_\rho)^2$. Subsequently, Burdman and Donoghue [4] suggested that the static b quark approximation may be valid over the entire q^2 range. Since measurement of $B \to (\rho, \omega)\gamma$ in the near future is unlikely, $B \to K^*\gamma$ is first related to $B \to (\rho, \omega)\gamma$ via SU(3) flavor symmetry, which in turn can be related to $B \to \rho l \nu$.

The modes $B^0 \to \rho^0\gamma$, $B^0 \to \omega\gamma$, and $B^- \to \rho^-\gamma$ are penguin decays similar to the $B \to K^*\gamma$ decays, but with a d quark in place of the s quark in the final state. Since the penguin loop contribution is dominated by the top quark, one can see that these $b \to d$ penguin decays should be related to the ordinary $b \to s$ penguin decays by a factor of $|V_{td}/V_{ts}|^2$. Although other issues come into play, including phase space, form factors, and long distance effects, the measurement of the $b \to d$ penguin modes still represents one of the best opportunities presently available to measure $|V_{td}/V_{ts}|$. ALEPH has used limits on B_s mixing [5] to set limits $|V_{td}/V_{ts}|$ with sensitivity comparable to ours.

In this paper we present new measurements of the $B \to K^*\gamma$ decay in four final states, $K^+\pi^-\gamma$, $K^0\pi^0\gamma$, $K^-\pi^0\gamma$, and $K^0\pi^-\gamma$. We also set 90% C.L. upper limits on the three decays, $\bar{B}^0 \to \omega\gamma$, $(\omega \to \pi^-\pi^+\pi^0)$, $\bar{B}^0 \to \rho^0\gamma$, $(\rho^0 \to \pi^-\pi^+)$, and $B^- \to \rho^-\gamma$, $(\rho^- \to \pi^-\pi^0)$.

II. DATA SET

The data used in this analysis were taken with the CLEO-II detector at the Cornell Electron Storage Ring (CESR). They consist of 2.40 fb^{-1} of integrated luminosity on the $\Upsilon(4S)$ resonance (2.57×10^6 $B\bar{B}$ events) and 1.14 fb^{-1} at a center-of-mass energy 60 MeV below the resonance.

The CLEO-II detector is a general purpose solenoidal detector designed to detect charged and neutral particles with high efficiency and good resolution [6]. Charged particles are tracked with three concentric cylindrical wire chambers operating in a 1.5 T magnetic field. The outer chamber (main drift chamber) provides charge particle identification via specific ionization (dE/dx) measurement. Further particle identification is achieved with a scintillation layer, Time of Flight (ToF), just outside the main drift chamber. An electromagnetic calorimeter is used for photon reconstruction. The calorimeter comprises 7800 CsI crystals positioned inside the magnet and has an excellent resolution of $\sigma_E/E = 2\%$ for $E \approx 2$ GeV in the central portion of the detector.

III. ANALYSIS

An in-depth discussion of analysis details may be found elsewhere [7]. We therefore restrict ourselves here to prominent features of the analysis.

A. Signal

We form a B candidate by combining a reconstructed meson (K^*, ρ, or ω) with a high energy photon. Charged tracks, photons, π^0's, and K_S's are selected according to standard procedures already in common use in CLEO's other rare B decay studies [8]. Wide cuts on the total energy and mass of the B candidate are applied to maximize the signal efficiency and to provide a signal-free region for background estimation. The candidate energy is most conveniently expressed by the quantity $\Delta E \equiv E_{candidate} - E_{beam}$. We compute the beam-constrained B-mass, M_B, by substituting the beam energy for the candidate energy thereby improving mass resolution. We retain for further analysis events in which there is a candidate lying in the region $5.2 < M_B < 5.3$ GeV and $|\Delta E|$ less than about 300 MeV. For $b \to d$ candidates we retain events with $5.274 < M_B < 5.286$ GeV and $|\Delta E| < 100$ MeV.

B. Background Suppression

The dominant backgrounds for this study arise from continuum $q\bar{q}$ production. We divide the continuum into two separate categories based on the origin of the high energy photon: from decay of π^0 or η in $q\bar{q}$ events ($Q\bar{Q}$) and from initial state radiation (ISR).

Once the candidates have been chosen, the event must pass a series of event shape cuts. Both B mesons in a $B\bar{B}$ event are produced approximately at rest in the lab frame. The decays of the two B mesons are therefore uncorrelated, producing a spherical event shape. In contrast, $Q\bar{Q}$ events tend to have a two-jet topology. ISR events lie between the two extremes. To exploit these differences, cuts are placed on the shape variables R_2, the second Fox-Wolfram moment [9], and $\cos\theta_{thrust}$, where θ_{thrust} is the angle between the photon's direction and the thrust axis of the rest of the event excluding the K, π, and γ candidates. We require $R_2 < 0.7$. The cut on $|\cos\theta_{thrust}|$ depends on mode, ranging from < 0.80 to 0.85 for the $K^*\gamma$ modes and from < 0.71 to 0.75 for the $(\rho,\omega)\gamma$ modes.

C. Additional Event Shape Criteria

To further exploit the shape differences between signal and the two backgrounds we use a Fisher discriminant. A Fisher discriminant [10,11] is a linear combination of several variables which individually may only marginally separate signal and background but taken together in optimal combination yield a variable which has good signal to background separation.

The set of input variables for the discriminant used in this analysis is similar to that used in other CLEO work. [8] The output from the Fisher discriminant for Monte Carlo samples of signal, $Q\bar{Q}$, and ISR is shown in Figure 1. To estimate possible systematic bias in the

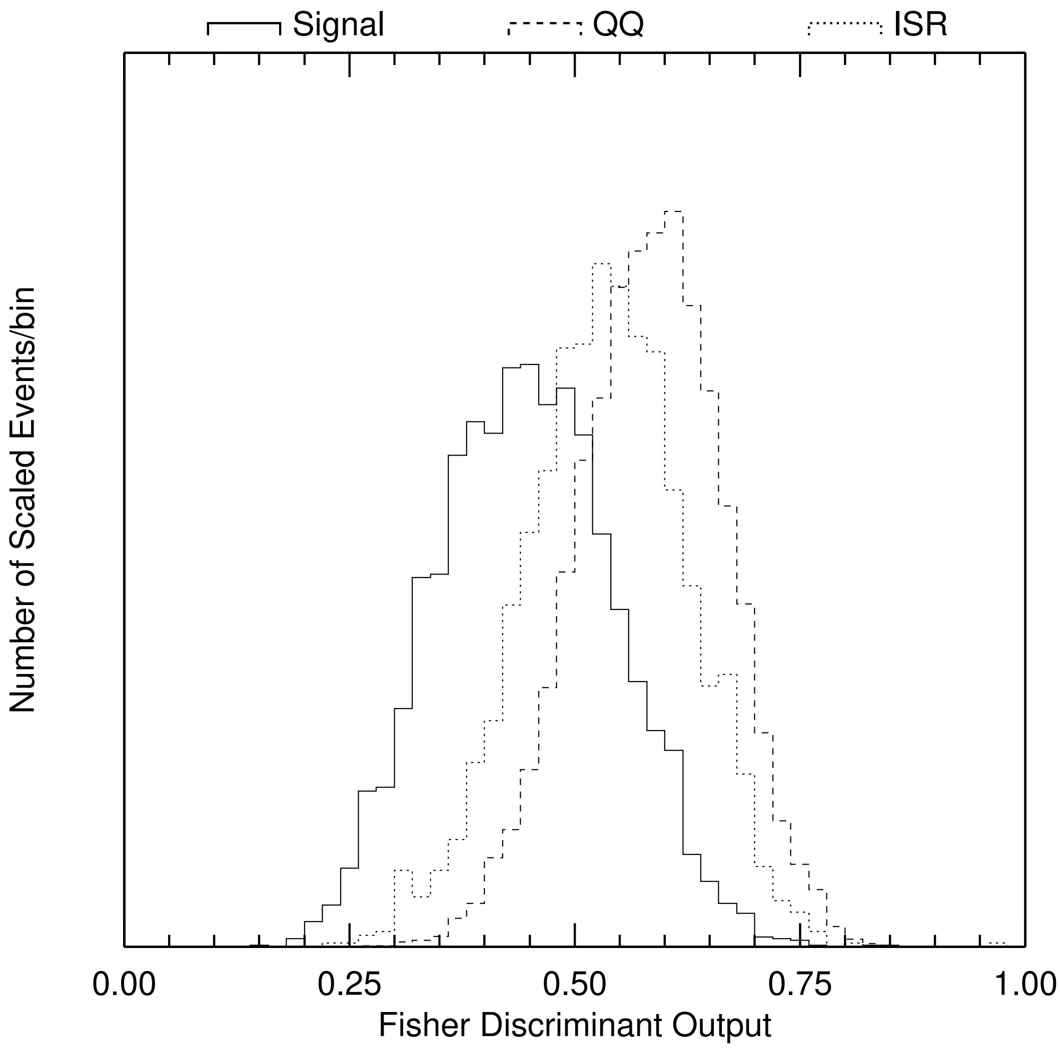

FIG. 1. The distribution of the Fisher discriminant output for Monte Carlo sample of $B^0 \to K^{*0}\gamma(K^{*0} \to K^+\pi^-)$ signal, $Q\bar{Q}$, and ISR are shown. The histograms have equal area and the x axis has been rescaled to make the Fisher discriminant output lie between 0 and 1.

measurement of Fisher discriminant between data and Monte Carlo events, we compared $B \to D\pi$ signal events as shown in Figure 2. The agreement is excellent.

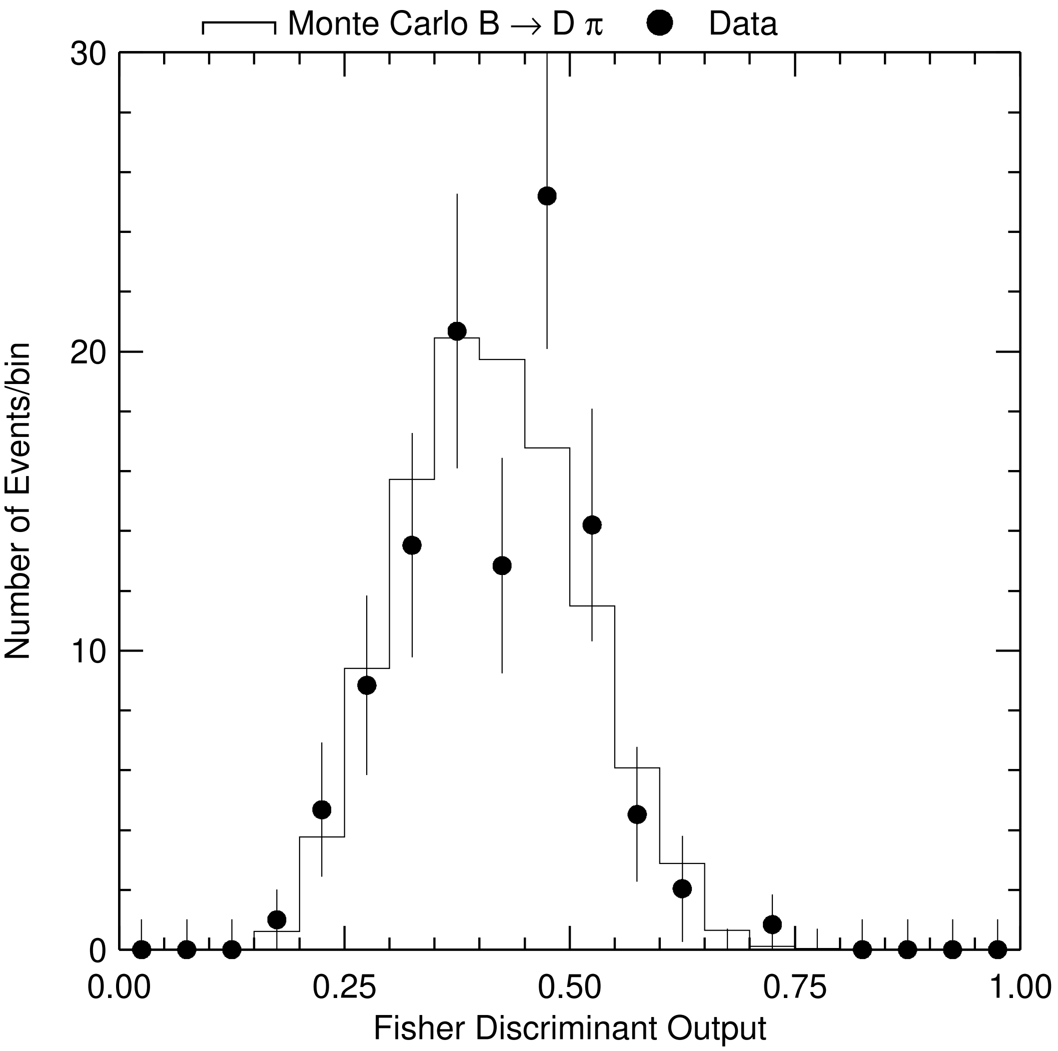

FIG. 2. Comparison between Fisher discriminant distributions for Monte Carlo and data $B \to D\pi$ signal events.

D. K^*/ρ Separation

While suppression of $Q\bar{Q}$ and ISR backgrounds suffices for the $K^*\gamma$ analysis, the $\rho\gamma$ analysis must take further steps to suppress background from $K^*\gamma$.

A neural network is used to distinguish $B^0 \to K^{*0}\gamma(K^{*0} \to K^+\pi^-)$ from $B^0 \to \rho^0\gamma$ events and $B^- \to K^{*-}\gamma(K^{*-} \to K^-\pi^0)$ from $B^- \to \rho^-\gamma$ events.

The neural network uses four inputs: $\Delta E_{\pi\pi}$, $M_{K\pi}$, $M_{\pi\pi}$, and $\cos\theta_\rho$. The masses $M_{K\pi}$ and $M_{\pi\pi}$ are calculated assuming the tracks are either a $K - \pi$ or $\pi - \pi$ pair. For the $B^- \to \rho^-\gamma$ case the assignment of the K mass is to the charged track. For the $B^0 \to \rho^0\gamma$ case we have two tracks, so the K mass is assigned to the track with the larger momentum. For $K^{*0} \to K^+\pi^-$ decays this will assign the K mass to the true kaon approximately two-thirds of the time. The angle θ_ρ is the decay angle of the ρ. The decay angle is found by transforming the momentum vector of the ρ's daughter with larger momentum, into the ρ's rest-frame, and then measuring the angle between the transformed momentum vector and the flight direction of the ρ in the lab frame.

Figure 3 shows the distribution of the neural network output for $B \to \rho\gamma$ and $B \to K^*\gamma$. The neural network output peaks at -1 for $B \to K^*\gamma$ events and at $+1$ for $B \to \rho\gamma$ events. Another feature of the neural network output is that the $B \to K^*\gamma$ distribution is bunched much closer to -1 than the $B \to \rho\gamma$ distribution is to $+1$. This is due to the fact that it is much easier to identify a K^* compared to a ρ, thanks to the narrower K^* width.

IV. RESULTS: $B \to K^*\gamma$

To better understand the relative amount of background in each of the $B \to K^*\gamma$ analyses, Figure 4 presents scatter plots of the selected events distributed on the ΔE and M_B plane. We refer to these plots as the Grand Side Band (GSB) since they are used to estimate the background in the signal region. The boxes shown in the Figure 4 denote the area most heavily populated by the signal events. We use a maximum likelihood method to determine signal and background yields, employing four variables: M_B, $M_{K\pi}$, ΔE, and the Fisher discriminant.

The $B \to K^*\gamma$ analyses contain a large fraction of background events. This is a consequence of our attempt to maximize the signal efficiency. The large Grand Side Band region is used by the maximum likelihood fit to determine the total amount of background in the data sample. By fixing the total amount of background in the GSB any excess events in the signal region will be attributed to $B \to K^*\gamma$ decays.

Another feature of Figure 4 is that the $B \to K^*\gamma$ decay modes containing a K^0 have substantially less background than those with a $K^\pm$. This arises because a $\pi^\pm$ can easily be mistaken for a $K^\pm$ at these momenta, and the majority of tracks in an event are pions. Therefore, we have much more fake $K^\pm$'s than K^0's.

Table I gives the results for the maximum likelihood fit in different $B \to K^*\gamma$ event samples. The maximum likelihood fit measures the fraction of signal in the event sample, f_{sig}, and the fraction of $Q\bar{Q}$ background relative to the total amount of background, $f_{Q\bar{Q}}$.

To better illustrate the signal content in the data, we make projection plots by applying

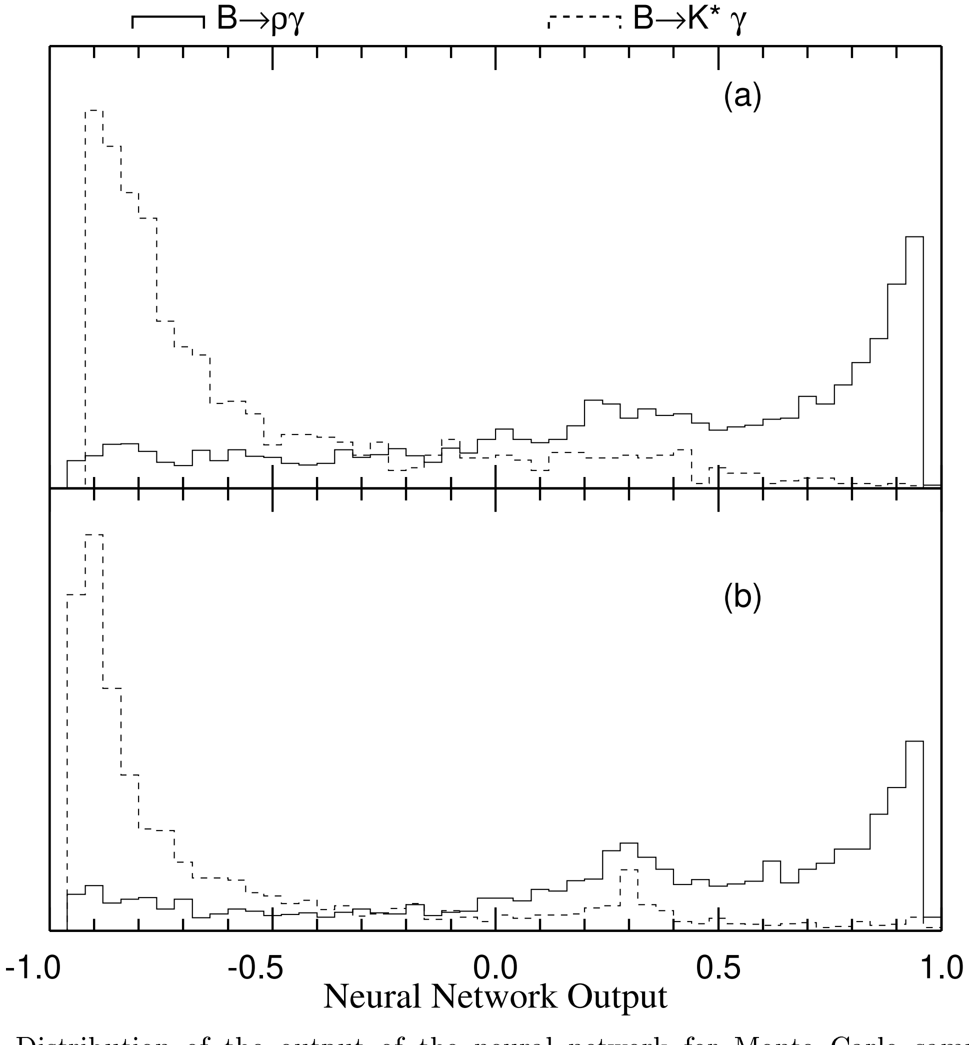

FIG. 3. Distribution of the output of the neural network for Monte Carlo samples of (a) $B^0 \to \rho^0\gamma$ and $B^0 \to K^{*0}\gamma(K^{*0} \to K^+\pi^-)$ and (b) $B^- \to \rho^-\gamma$ and $B^- \to K^{*-}\gamma(K^{*-} \to K^-\pi^0)$.

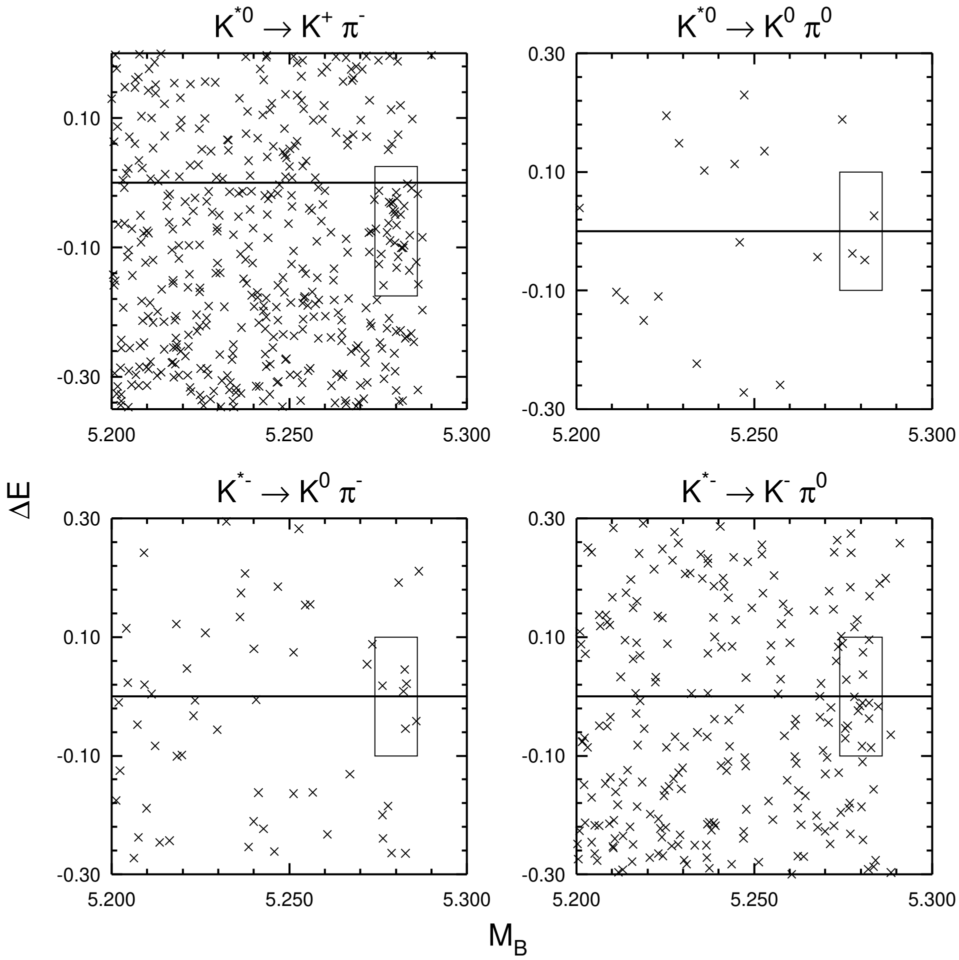

FIG. 4. Distribution of $B \to K^{*}\gamma$ events in the M_B and ΔE plane.

TABLE I. Maximum Likelihood Fit Results

	$K^{*0} \to K^+\pi^-$	$K^{*0} \to K^0\pi^0$	$K^{*-} \to K^0\pi^-$	$K^{*-} \to K^-\pi^0$
Events in fit	420	20	58	234
f_{sig}	$0.057^{+0.014}_{-0.012}$	$0.14^{+0.09}_{-0.07}$	$0.11^{+0.05}_{-0.04}$	$0.020^{+0.015}_{-0.011}$
$f_{Q\bar{Q}}$	0.81 ± 0.06	$1.0^{+0.0}_{-0.2}$	$0.75^{+0.19}_{-0.20}$	0.68 ± 0.10

restrictive selection criteria on three of the four maximum likelihood variables and projecting the remaining events onto the axis of the fourth variable. For example, the events shown in the ΔE projection are required to pass restrictive selection criteria for M_B, $M_{K\pi}$ and the Fisher discriminant output. Figures 5, 6, 7, and 8 show the projection plots for the $B \to K^*\gamma$ decays. Superimposed on the data histograms are the results from the maximum likelihood fits, where the curves have been rescaled to account for the efficiency loss due to the additional selection criteria.

Several observations about the data can be made from the projection plots. The first observation is that all the projection plots show strong indications of signal. The signal can most easily be discerned in the M_B projections. The second observation is the projection of the Fisher discriminant output appears to be shifted to the low end when compared to the fit curve. This shift is away from the area populated by the $Q\bar{Q}$ and ISR background. This shift explains the large estimated systematic bias shown in Section IV B when using different shapes for the Fisher discriminant distribution. Also note that there appears to be poor agreement among the projected events and the superimposed fit for the $B^- \to K^{*-}\gamma(K^{*-} \to K^-\pi^0)$ plots. In the $B^- \to K^{*-}\gamma(K^{*-} \to K^-\pi^0)$ M_B projection, the number of signal events appears to be much larger than what is seen in the fit, while the other projections either have ambiguous signal or, for the Fisher discriminant output, a preponderance of background. The maximum likelihood fit has found the best compromise among the competing projections. The compromise is not very unique which is reflected in the large fit error shown in Table I. The $B^- \to K^{*-}\gamma(K^{*-} \to K^-\pi^0)$ maximum likelihood fit is also quite sensitive to the precise shape of the M_B signal distribution. The sensitivity to the M_B shape is addressed in Section IV B.

TABLE II. Individual $B \to K^*\gamma$ Branching Fractions

Decay Mode	Signal Events	Efficiency (%)	Branching Fraction ($\times 10^{-5}$)
$K^{*0} \to K^+\pi^-$	$24.2^{+6.1}_{-5.6}$	22.3 ± 2.0	$4.2^{+1.1}_{-1.0} \pm 0.4$
$K^{*0} \to K^0\pi^0$	$2.8^{+2.0}_{-1.5}$	1.8 ± 0.2	$6.1^{+4.2}_{-3.3} \pm 0.8$
$K^{*-} \to K^0\pi^-$	$6.3^{+3.0}_{-2.5}$	5.7 ± 0.6	$4.3^{+2.1}_{-1.7} \pm 0.5$
$K^{*-} \to K^-\pi^0$	$4.6^{+4.4}_{-3.0}$	6.9 ± 0.7	$2.6^{+2.5}_{-1.7} \pm 0.3$

Table II shows the values used to calculate the branching fractions for the different $B \to K^*\gamma$ decay modes. The first error assigned to the branching fraction measurement

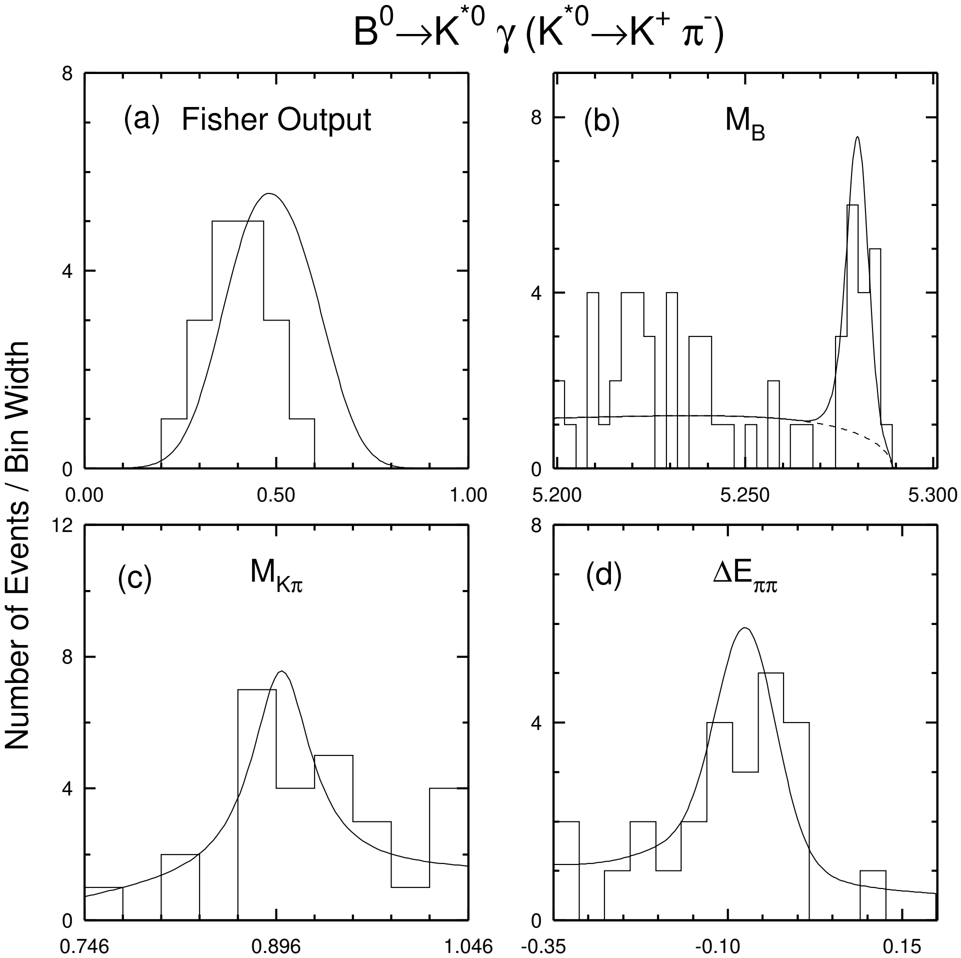

FIG. 5. Projection of $B^0 \to K^{*0}\gamma(K^{*0} \to K^+\pi^-)$ data events and maximum likelihood fits onto the four fit variables:(a) Fisher discriminant output, (b)M_B, (c) $M_{K\pi}$, and (d) $\Delta E_{\pi\pi}$.

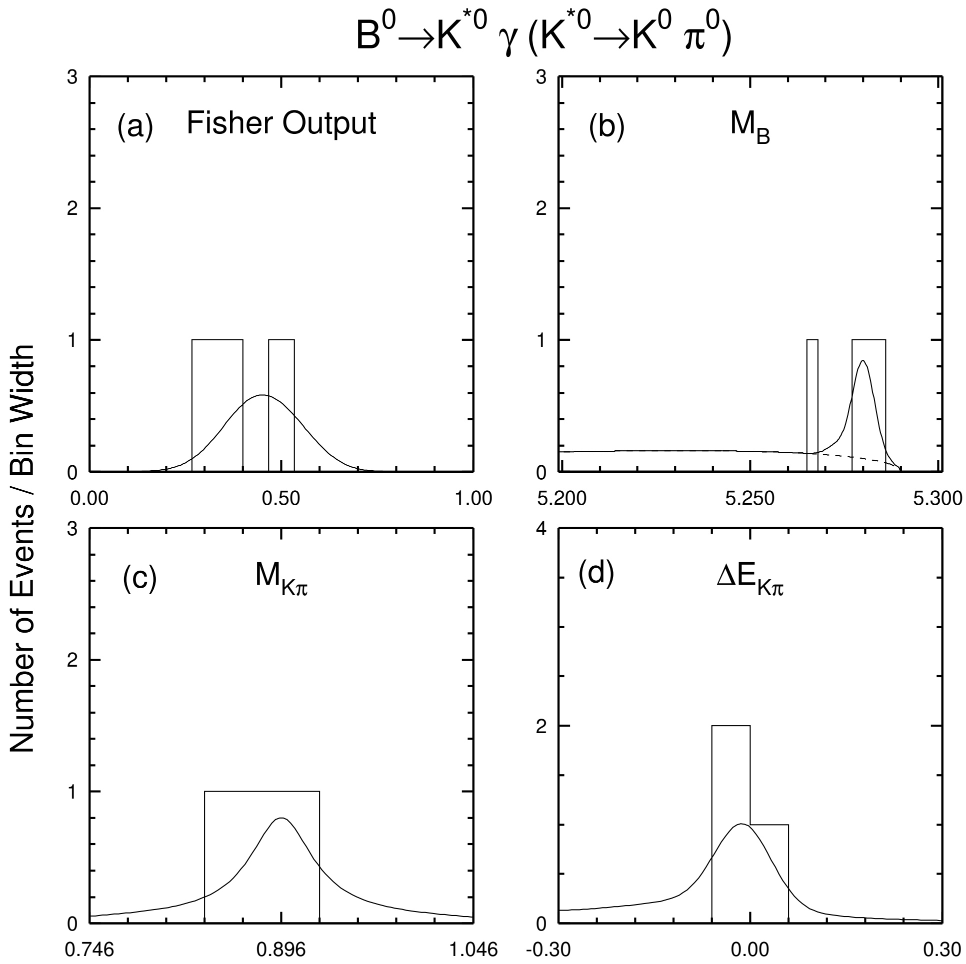

FIG. 6. Projection of $B^0 \to K^{*0}\gamma(K^{*0} \to K^0\pi^0)$ data events and maximum likelihood fits onto the four fit variables:(a) Fisher discriminant output, (b)M_B, (c) $M_{K\pi}$, and (d) $\Delta E_{K\pi}$.

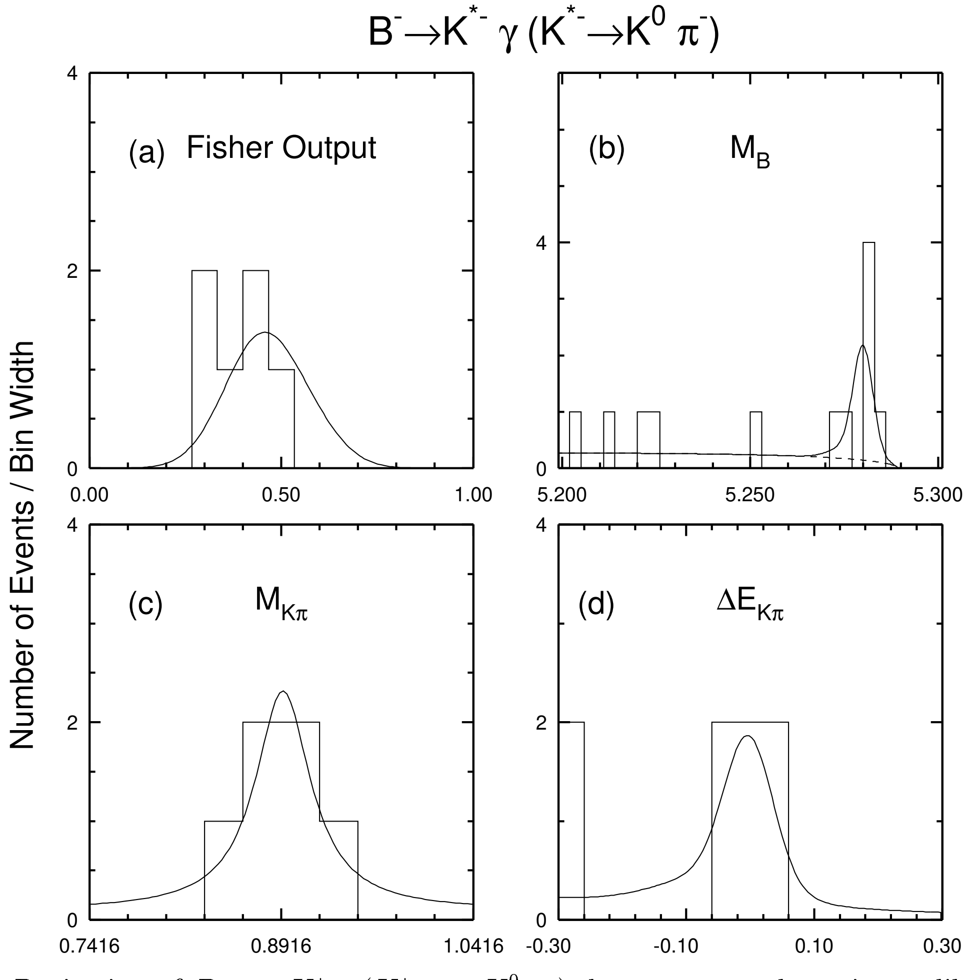

FIG. 7. Projection of $B^- \to K^{*-}\gamma(K^{*-} \to K^0\pi^-)$ data events and maximum likelihood fits onto the four fit variables:(a) Fisher discriminant output, (b)M_B, (c) $M_{K\pi}$, and (d) $\Delta E_{K\pi}$.

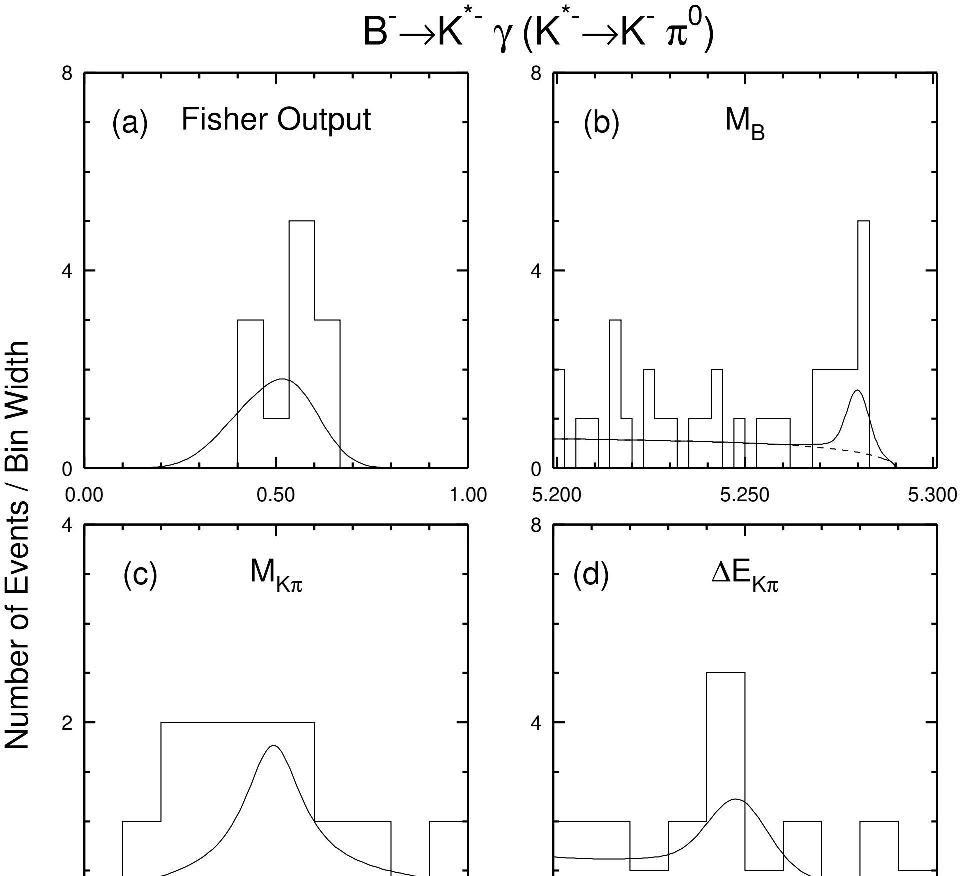

FIG. 8. Projection of $B^- \to K^{*-}\gamma(K^{*-} \to K^-\pi^0)$ data events and maximum likelihood fits onto the four fit variables:(a) Fisher discriminant output, (b)M_B, (c) $M_{K\pi}$, and (d) $\Delta E_{K\pi}$.

is from the total maximum likelihood fit error (statistical and systematic errors added in quadrature), while the second is from the error on the efficiency.

Table III lists the branching fractions obtained by combining the branching fractions from related $B \to K^*\gamma$ modes and compares them to the previous CLEO measurement [1]. The

TABLE III. Combined $B \to K^*\gamma$ Branching Fractions

Decay Mode	Branching Fraction ($\times 10^{-5}$) New	Previous
$B^0 \to K^{*0}\gamma$	$4.4 \pm 1.0 \pm 0.6$	$4.0 \pm 1.7 \pm 0.8$
$B^- \to K^{*-}\gamma$	$3.8^{+2.0}_{-1.7} \pm 0.5$	$5.7 \pm 3.1 \pm 1.1$
$B \to K^*\gamma$	$4.2 \pm 0.8 \pm 0.6$	$4.5 \pm 1.5 \pm 0.9$

branching fraction for $B^0 \to K^{*0}\gamma$ combines the branching fractions for $B^0 \to K^{*0}\gamma(K^{*0} \to K^+\pi^-)$ and $B^0 \to K^{*0}\gamma(K^{*0} \to K^0\pi^0)$. Likewise the $B^- \to K^{*-}\gamma$ branching fraction is obtained by combining $B^- \to K^{*-}\gamma(K^{*-} \to K^0\pi^-)$ and $B^- \to K^{*-}\gamma(K^{*-} \to K^-\pi^0)$. The final branching fraction for $B \to K^*\gamma$ is formed from $B^0 \to K^{*0}\gamma$ and $B^- \to K^{*-}\gamma$.

From Table III we see that our new $B \to K^*\gamma$ branching fractions are in good agreement with previous CLEO results. Several factors contribute to the smaller errors quoted on the new measurement. The new measurement uses 85% more data, and the efficiency for each mode is at least double that of the previous method. The doubling of the efficiency is due to the use of the maximum likelihood fit combined with the loose selection criteria. Because of the smaller statistical uncertainties, we have also conducted a more detailed study of the systematic uncertainties.

A. $\Gamma(B \to K^*\gamma)/\Gamma(b \to s\gamma)$ Measurement

We combine our new $B \to K^*\gamma$ branching fraction measurement with CLEO's previous measurement [12] of

$$Br(b \to s\gamma) = (2.32 \pm 0.57 \pm 0.35) \times 10^{-4},$$

to get the ratio

$$\frac{\Gamma(B \to K^*\gamma)}{\Gamma(b \to s\gamma)} = 0.181 \pm 0.068.$$

Table IV lists a selection of theoretical estimates on this ratio. These estimates range from 4 to 40%. The discrepancy between theoretical estimates is largely due to different methods of calculating the non-perturbative QCD effects.

TABLE IV. Theoretical Estimates of $\Gamma(B \to K^* \gamma)/\Gamma(b \to s\gamma)$

Reference	Ratio (%)
Altomari [13] (1988)	4.5
Deshpande *et al.* [14] (1988)	7
Dominguez *et al.* [15] (1988)	28 ± 11
Deshpande & Trampetic [16] (1989)	6-14
Aliev *et al.* [17] (1990)	39
Ali & Mannel [18] (1991)	18-28
Faustov & Galkin [19] (1992)	6.5
Ali, Ohl,& Mannel [20] (1993)	3.5-12.2
El hassan & Riazuddin [21] (1993)	7-10
Colangelo *et al.* [22] (1993)	17 ± 5
O'Donnell & Tung [23] (1993)	10
Ali & Greub [24] (1993)	13
Ball [25] (1993)	20 ± 6
Ali, Braun & Simma [26] (1994)	16 ± 5
Bernard, Hsieh & Soni [27] (1994)	$6.1 \pm 1.1 \pm 3.4$
Holdom & Sutherland [28] (1994)	17 ± 4
Narison [29] (1994)	16 ± 4
Bowler *et al.* [30] (1994)	$9 \pm 3 \pm 1$
Ciuchini *et al.* [31] (1994)	23 ± 9
Tang *et al.* [32] (1995)	$10 - 12$

B. Systematic Uncertainties

There are three dominant sources of systematic uncertainties in the $K^*\gamma$ analysis: the efficiency calculation, backgrounds from $B\bar{B}$ decays, and the maximum likelihood fit. The largest uncertainties arise from the uncertainty on the M_B and Fisher discriminant shapes used in the maximum likelihood fit. Table V summarizes the results from the systematic studies. We note that the $K^{*-} \to K^-\pi^0$ mode has substantially larger systematic uncertainty from maximum likelihood fit as described above.

TABLE V. $B \to K^*\gamma$ Systematic Bias Estimation Summary

Decay Mode	Efficiency	Maximum Likelihood $B\bar{B}$ Decays	Fit	Combined
$K^{*0} \to K^+\pi^-$	8.8	$^{+0.1}_{-1.6}$	$^{+7.8}_{-8.2}$	$^{+7.8}_{-8.4}$
$K^{*0} \to K^0\pi^0$	12.6	$^{+0.0}_{-0.8}$	$^{+6.5}_{-3.7}$	$^{+6.5}_{-3.8}$
$K^{*-} \to K^0\pi^-$	10.6	0.0	$^{+11.7}_{-11.8}$	$^{+11.7}_{-11.8}$
$K^{*-} \to K^-\pi^0$	10.0	$^{+0.0}_{-6.1}$	$^{+59.4}_{-23.9}$	$^{+59.4}_{-24.7}$

V. RESULTS: $B \to (\rho, \omega)\gamma$

Because of the smallness of the candidate sample, we extract signal in the $B \to (\rho, \omega)\gamma$ analysis differently than in the $B \to K^*\gamma$ analysis. We make specific cuts in the variables that separate the signal from the background, instead of the maximum likelihood method. Figure 9 shows the ΔE and M_B scatter plots of the events that pass all cuts. The box shown in each figure indicates the signal region.

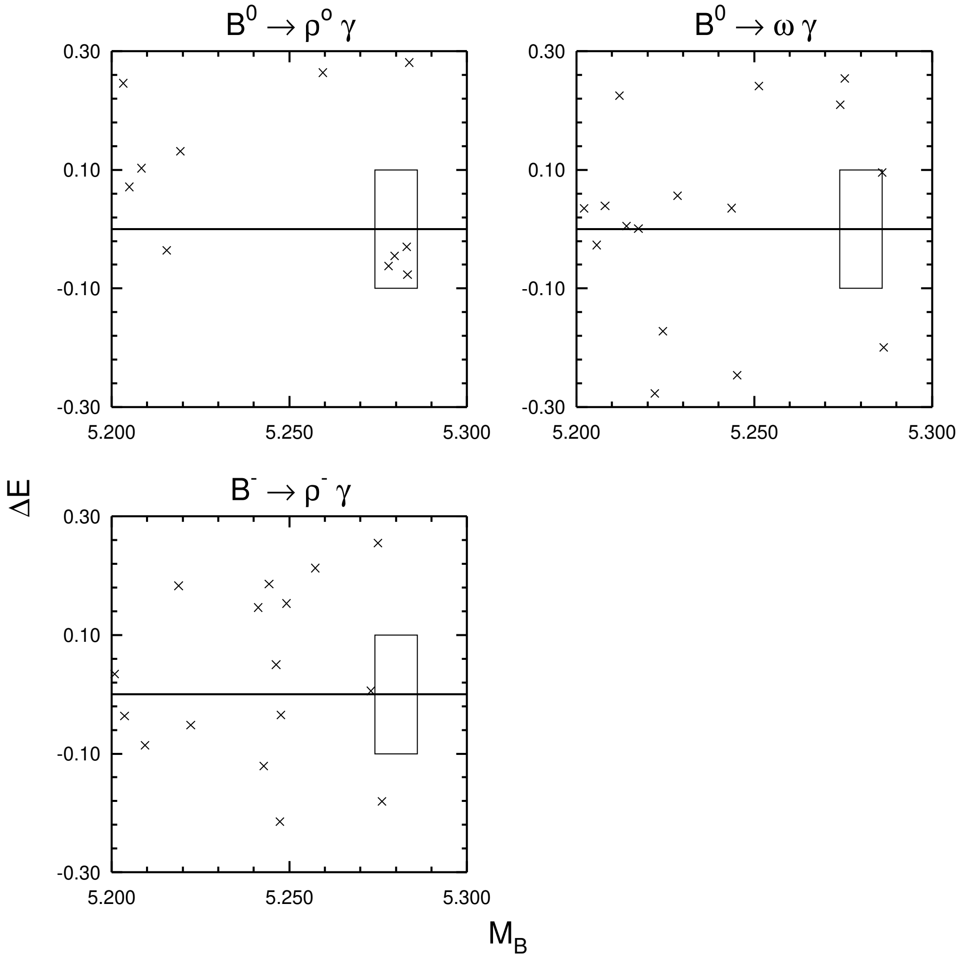

FIG. 9. Distribution of $B \to (\rho, \omega)\gamma$ events in the M_B and ΔE plane.

To better visualize the total amount of $Q\bar{Q}$ and ISR background that could be in the signal region, M_B projections for the $B \to (\rho, \omega)\gamma$ decay modes are shown in Figure 10. These projections include the final $|\Delta E| < 100$ MeV requirement. Table VI list the number of events which lie within the signal regions for the $B \to (\rho, \omega)\gamma$ analysis as well as the expected number of background events. The number of $Q\bar{Q}$ and ISR background events is estimated by scaling the $Q\bar{Q}$ and ISR Monte Carlo to match the number of data events in the Grand Side Band. The scaling assumes that the data in the Grand Side Band is $(80 \pm 10)\%$ $Q\bar{Q}$ events based on relative $\Upsilon(4S)$ and continuum cross sections. We estimate the $B \to K^*\gamma$ background by scaling $B \to K^*\gamma$ Monte Carlo assuming $Br(B \to K^*\gamma) = 4.5 \times 10^{-5}$. The error reported for the background sum takes into account the correlation between the $Q\bar{Q}$

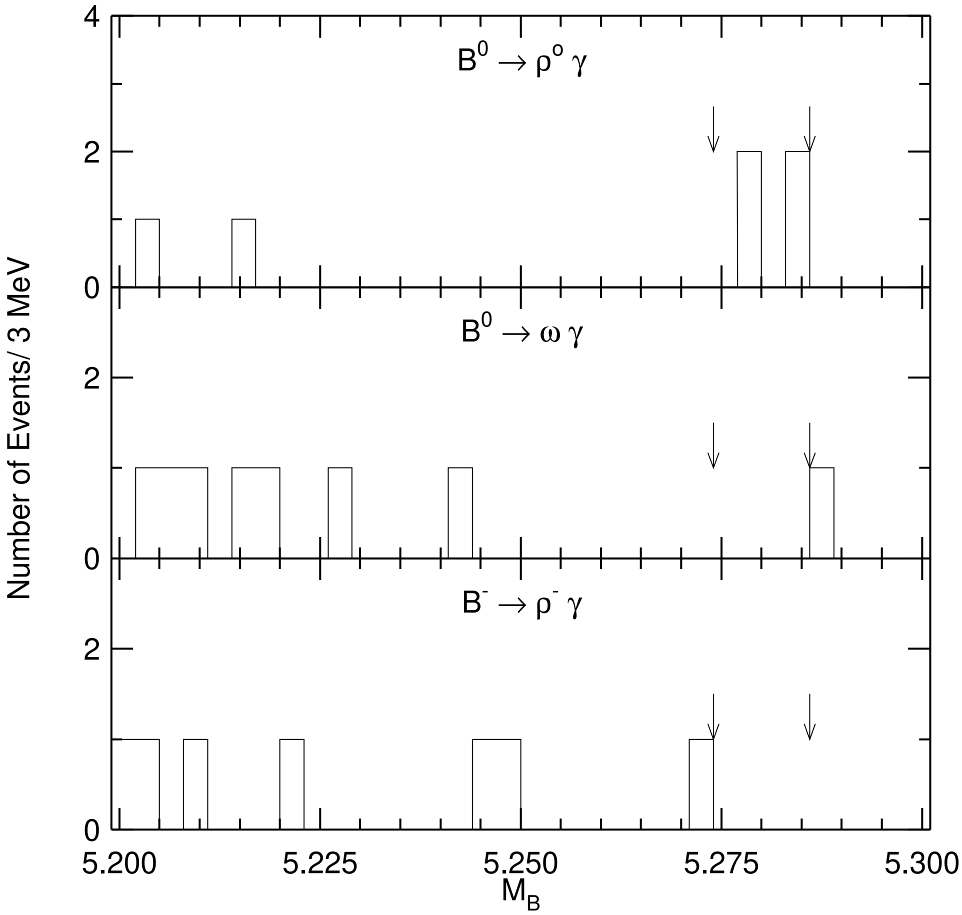

FIG. 10. Projection of $B \to (\rho, \omega)\gamma$ data events onto the M_B axis.

TABLE VI. Events in $B \to (\rho, \omega)\gamma$ Analyses

	$B^0 \to \rho^0\gamma$	$B^0 \to \omega\gamma$	$B^- \to \rho^-\gamma$
Events in Signal Region	4	0	0
QQ background	0.23 ± 0.08	0.56 ± 0.18	0.40 ± 0.11
ISR background	0.18 ± 0.12	0.14 ± 0.10	0.12 ± 0.09
$B \to K^*\gamma$ background	0.45 ± 0.11	0.0	0.27 ± 0.06
Background sum	0.85 ± 0.17	0.70 ± 0.14	0.79 ± 0.14

and ISR background estimates. The background estimates are not used when calculating the upper limits and are only provided to show the size of possible background contamination.

No events lie within the signal region for $B^0 \to \omega\gamma$ and $B^- \to \rho^-\gamma$, but four events are in the signal region for $B^0 \to \rho^0\gamma$. A closer look at the properties of the four events in $B^0 \to \rho^0\gamma$ shows that they do not pose compelling evidence for a $B^0 \to \rho^0\gamma$ signal. Figure 9 shows that all the events in the signal region fall on the low side of ΔE which is the area populated by events from $B^0 \to K^{*0}\gamma(K^{*0} \to K^+\pi^-)$. In addition, Figure 11 shows that the neural network output from the four events lie near the selection criterion for the neural network. A strong $B^0 \to \rho^0\gamma$ signal would have had events near +1 (See Figure 3). The selection criteria were chosen purely on the basis of Monte Carlo studies.

A. Branching Fraction Upper Limits

We combine the information presented in the previous section with the efficiency measurements presented earlier to calculate the upper limits on the $B \to (\rho, \omega)\gamma$ branching fractions. These values are compared to previous CLEO measurements and to theoretical estimates. The following sections use these branching fraction measurements to extract measurements on theoretically interesting physical quantities.

The errors quoted on the efficiencies are the total error on that quantity. This total error is the quadratic sum of the statistical and systematic errors.

TABLE VII. $B \to (\rho, \omega)\gamma$ Branching Fraction Upper Limits

Decay Mode	Signal Events	Efficiency (%)	Branching Fraction ($\times 10^{-5}$)
$B^0 \to \rho^0\gamma$	4 (7.99)	9.2 ± 1.3	< 3.9
$B^0 \to \omega\gamma$	0 (2.30)	8.9 ± 1.2	< 1.3
$B^- \to \rho^-\gamma$	0 (2.30)	9.2 ± 1.3	< 1.1

Table VII shows the values used in calculating the upper limit on the $B \to (\rho, \omega)\gamma$ branching fractions. The number in parenthesis next to the number of events in the signal region is the 90% Poisson upper limit for measuring that many events. The error on the

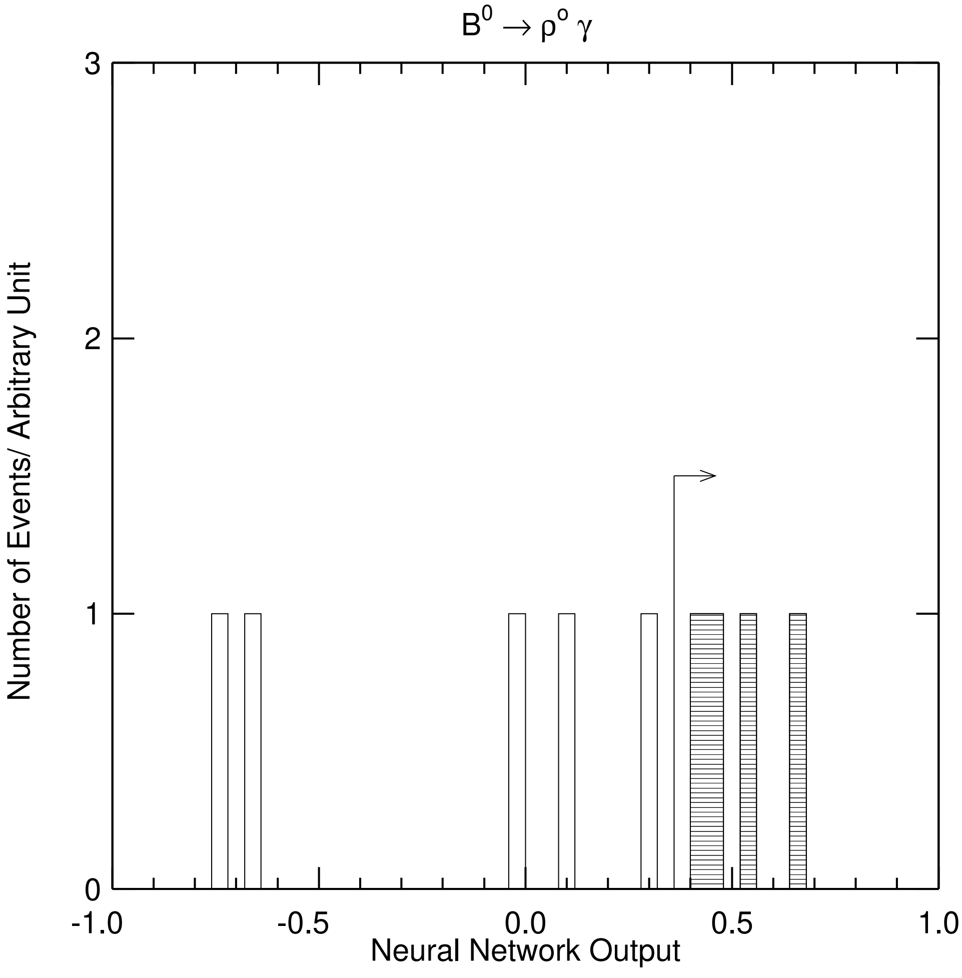

FIG. 11. Projection of $B^0 \to \rho^0\gamma$ data events onto the neural network output axis. The arrow shows the minimum neural network output selection criteria and the shaded events are those which pass this selection.

efficiency value is the total error which is dominated by the systematic uncertainty. To account for the systematic uncertainty in the upper limit calculation, we have increased the value of the upper limit by the magnitude of the systematic uncertainty.

Table VIII lists theoretical estimates of $Br(B^- \to \rho^-\gamma)$. Only $B^- \to \rho^-\gamma$ branching ratios are quoted since if we ignore any long distance effects the $B \to (\rho,\omega)\gamma$ decays are expected to obey the relationship

$$\Gamma(B^- \to \rho^-\gamma) = 2\Gamma(B^0 \to \rho^0\gamma) = 2\Gamma(B^0 \to \omega\gamma).$$

The factor of 2 accounts for the likelihood that the quark pair $d\bar{d}$ (from $B^0 \to (d\bar{d})\gamma$) will form a ρ^0 or an ω. Comparing the values shown in Table VIII to the results in Table VII we see that the theoretical estimates are still approximately an order of magnitude smaller than our upper limits.

TABLE VIII. Theoretical Estimates for $Br(B^- \to \rho^-\gamma)$

Reference	Branching Fraction ($\times 10^{-5}$)
Soares [33]	0.04 – 0.7
Greub *et al.* [34]	0.12 – 0.30

B. $|V_{td}/V_{ts}|$ Measurement

The ratio of $Br(B \to K^*\gamma)$ to $Br(B \to (\rho,\omega)\gamma)$ is related to the ratio of CKM matrix elements $|V_{td}/V_{ts}|$. If we ignore contributions due to long distance effects then we get the approximate relationship

$$\frac{Br(B^- \to \rho^-\gamma)}{Br(B^- \to K^{*-}\gamma)} = \frac{Br(B^0 \to \rho^0\gamma) + Br(B^0 \to \omega\gamma)}{Br(B^0 \to K^{*0}\gamma)} = \left|\frac{V_{td}}{V_{ts}}\right|^2 \xi\Omega. \tag{1}$$

Where the term ξ accounts for $SU(3)$ symmetry breaking and Ω represents the phase space ratio.

By assuming $Br(B^0 \to K^{*0}\gamma) = Br(B^- \to K^{*-}\gamma)$ we can combine the three $B \to (\rho,\omega)\gamma$ modes to determine the upper limit

$$\frac{Br(B \to (\rho,\omega)\gamma)}{Br(B \to K^*\gamma)} < 0.19.$$

The value for $Br(B \to (\rho,\omega)\gamma)$ is calculated from the 90 % confidence upper limit on observing 4 events in $B^0 \to \rho^0\gamma$, 0 events in $B^0 \to \omega\gamma$, and 0 events in $B^- \to \rho^-\gamma$ given that the expected numbers of events, μ_x, are related by

$$\frac{2\mu_{\rho^0}}{\epsilon_{\rho^0}} = \frac{2\mu_\omega}{\epsilon_\omega} = \frac{\mu_{\rho^-}}{\epsilon_{\rho^-}}. \tag{2}$$

where ϵ_x is the efficiency of the x decay mode. Using a Monte Carlo technique we found $\mu_{\rho^-} = 1.52$. Combining μ_{ρ^-} with the efficiency for $B^- \to \rho^-\gamma$ and $Br(B \to K^*\gamma)$ gives the upper limit. The upper limit on the ratio of branching fractions has been scaled up by a factor of 1.22 to account for the efficiency and maximum likelihood fit total errors.

To determine an upper limit on $|V_{td}/V_{ts}|$, we need estimates on the values of Ω and ξ from Equation 1. The phase space factor Ω is given by [26]

$$\begin{aligned}\Omega &= \frac{(m_b^2 + m_d^2)}{(m_b^2 + m_s^2)} \frac{(m_B^2 - m_\rho^2)^3}{(m_B^2 - m_{K^*}^2)^3}, \\ &= 1.02 \pm 0.02.\end{aligned} \tag{3}$$

To calculate Ω we use the quark masses $m_b = 5.0$ GeV, $m_s = 300$ MeV, and $m_d = 100$ MeV. The uncertainty on Ω comes from using a value of $m_b = 4.5$ GeV to test the sensitivity of Ω from m_b. With the above value of Ω, we set an upper limit on the product quantity,

$$\left|\frac{V_{td}}{V_{ts}}\right|^2 \xi < 0.19. \tag{4}$$

The SU(3) symmetry breaking term, ξ, has been estimated by different theoretical techniques. Table IX lists the various calculations for ξ and the upper limit on $|V_{td}/V_{ts}|$ obtained using those values.

TABLE IX. Constraints on $|V_{td}/V_{ts}|$

Reference	Model	ξ	Upper Limit
Ali *et al.* [26]	QCD Sum Rule	0.58	< 0.56
Soares [33]	BSW Formalism	0.72 - 0.90	$< 0.45 - 0.50$
Narison [29]	Hybrid QCD Sum Rule	0.77	< 0.49

C. $|V_{td}/V_{ts}|$ Systematic Uncertainty

We expect some cancelation of the efficiency systematic uncertainties between the numerator and the denominator. To estimate this cancelation, we take the difference of the sum of the numerator and denominator efficiency systematics. In the sum, all the $B \to K^*\gamma$ modes count for 1/4 whereas $B^0 \to \omega\gamma$ and $B^0 \to \rho^0\gamma$ are 1/4 but $B^- \to \rho^-\gamma$ counts for 1/2. For example, all the modes are susceptible to the systematic uncertainty on the photon selection, whereas only the $B^0 \to \omega\gamma$, $B^- \to \rho^-\gamma$, $B^0 \to K^{*0}\gamma(K^{*0} \to K^0\pi^0)$, and $B^- \to K^{*-}\gamma(K^{*-} \to K^-\pi^0)$ modes are sensitive to the π^0 efficiency. Therefore, these two uncertainties contribute to the total uncertainty on the ratio as

$$\begin{aligned}\sigma_{total}^2 &= (\sigma_\gamma(1-1))^2 + (\sigma_{\pi^0}(\frac{1}{4} + \frac{1}{2} - \frac{1}{4} - \frac{1}{4}))^2 + \ldots, \\ &= \frac{1}{16}\sigma_{\pi^0}^2 + \ldots .\end{aligned} \tag{5}$$

The final efficiency systematic uncertainty is 9.6%. This is combined in quadrature with the 19.5% systematic uncertainty on the $B \to K^* \gamma$ maximum likelihood fit to yield a total uncertainty on $|V_{td}/V_{ts}|$ of 22%.

VI. CONCLUSION

With 2.6×10^6 $B\bar{B}$ events collected by the CLEO II detector, we have made new measurements of the $B^0 \to K^{*0}\gamma(K^{*0} \to K^+\pi^-)$, $B^0 \to K^{*0}\gamma(K^{*0} \to K^0\pi^0)$, $B^- \to K^{*-}\gamma(K^{*-} \to K^0\pi^-)$, and $B^- \to K^{*-}\gamma(K^{*-} \to K^-\pi^0)$ branching fractions. We also combine the branching fraction for $B \to K^*\gamma$ with the recent CLEO collaboration inclusive measurement of $b \to s\gamma$ to determine the exclusive to inclusive decay width ratio.

Our limit on $|V_{td}/V_{ts}| < 0.45 - 0.56$, can be compared to the recent ALEPH limit [5] obtained from B_s^0 Oscillation. We expect a steady improvement in the CLEO limit in the next few years with luminosity upgrades of CESR.

ACKNOWLEDGEMENTS

We gratefully acknowledge the effort of the CESR staff in providing us with excellent luminosity and running conditions. J.P.A., J.R.P., and I.P.J.S. thank the NYI program of the NSF, M.S thanks the PFF program of the NSF, G.E. thanks the Heisenberg Foundation, K.K.G., M.S., H.N.N., T.S., and H.Y. thank the OJI program of DOE, J.R.P, K.H., and M.S. thank the A.P. Sloan Foundation, and A.W., and R.W. thank the Alexander von Humboldt Stiftung for support. This work was supported by the National Science Foundation, the U.S. Department of Energy, and the Natural Sciences and Engineering Research Council of Canada.

REFERENCES

[1] R. Ammar *et al.* (CLEO Collaboration), Evidence for Penguin-Diagram Decays: First Observation of $B \to K^*(892)\gamma$, *Phys. Rev. Lett.* **71**, 674 (1993).

[2] A. J. Buras, Theoretical Review of B-Physics, *Nucl. Instrum. Meth.* A **361**, 1 (1995).

[3] N. Isgur and M.B. Wise, Relationship between form factors in semileptonic $\bar{B}$ and D decays and exclusive rare $\bar{B}$-meson decays, *Phys. Rev.* D **42**, 2388 (1990).

[4] G. Burdman and J.F. Donoghue, Reliable predictions in exclusive rare B decays, *Phys. Lett.* B **270**, 55 (1991).

[5] D. Buskulic *et al.* (ALEPH Collaboration), Limit on B_s^0 Oscillation Using a Jet Charge Method, *Phys. Lett.* B **356**, 409 (1995). From the time dependent study of B_s^0 oscillation, they have set an upper limit, $|V_{td}/V_{ts}| < 0.37-0.42$ where the range is due to uncertainty in f_{B_s}.

[6] Y. Kubota et al. (CLEO Collaboration), The CLEO-II detector, *Nucl. Instrum. Meth.* A **320**, 66 (1992).

[7] C.D. Jones, Measurement of Exclusive Electromagnetic Penguin Decays of the B Mesons, PhD Thesis, Cornell University, 1996.

[8] D.M. Asner *et al.* (CLEO Collaboration), Search for Exclusive Charmless Hadronic B Decays, *Phys. Rev.*, D **53**, 1039 (1996).

[9] G. Fox and S. Wolfram, Observables for the Analysis of Event Shapes in $e^+ e^-$ Annihilation and Other Processes, *Phys. Rev. Lett.* **41**, 1581 (1978).

[10] R. A. Fisher, The Use of Multiple Measurements in Taxonomic Problems, *Annals of Eugenics* **7**, 179 (1936).

[11] M.G. Kendall and A. Stuart, *The Advanced Theory of Statistics*, Volume III, Hafner Publishing, NY, 2nd edition, 1968.

[12] M. S. Alam *et al.* (CLEO Collaboration), First Measurement of the Rate for the Inclusive Radiative Penguin Decay $b \to s\gamma$, *Phys. Lett.* **74**, 2885 (1995).

[13] T. Altomari, Contribution of Exclusive Decays $B \to K^{**}\gamma$ to $b \to s\gamma$, *Phys. Rev.* D **37**, 677 (1988).

[14] N.G. Deshpande *et al.*, Flavor Changing Radiative B Decays, *Z. Phys.* C **40**, 369 (1988).

[15] C.A. Dominguez *et al.*, Rare Decay $B \to K^*\gamma$ in the Standard Model, *Phys. Lett.* B **214**, 459 (1988).

[16] N.G. Deshpande and J. Trampetic, Electromagnetic Penguins in B Decays, *Ann. N.Y. Acad. Sci.*, **578**, 424 (1989).

[17] T.M. Aliev *et al.*, Rare Decay $B \to K^*\gamma$ in Standard and Supersymmetric Models, *Phys. Lett.* B **237**, 569 (1990).

[18] A. Ali and T. Mannel, Exclusive Rare B Decays in the Heavy Quark Limit, *Phys. Lett.* B **264**, 447 (1991).

[19] R.N. Faustov and V.O. Galkin, Rare Decay $B \to K^*\gamma$ in the Relativistic Quark Model, *Mod. Phys. Lett.* A **7**, 2111 (1992).

[20] A. Ali, T. Ohl, and T. Mannel, Radiative Rare B Decays into Higher K Resonances, *Phys. Lett.* B **298**, 195 (1993).

[21] El hassan El aaoud and Riazuddin, Flavor Changing Radiative B Decays and Flavor Conserving Radiative Decays of Ground State Mesons, *Phys. Rev.* D **47**, 1026 (1993).

[22] P. Colangelo *et al.*, Radiative $B \to K^*\gamma$ transition in QCD, *Phys. Lett.* B **317**, 183 (1993).

[23] P.J. O'Donnell and H.K.K. Tung, The Rare Decay $B \to K^*\gamma$: A More Precise Calculation, *Phys. Rev.* D **48**, 2145 (1993).

[24] A. Ali and C. Greub, A Determination of the CKM Matrix Element Ratio $|V_{ts}/V_{cb}|$ from the Rare B Decays $B \to K^* + \gamma$ and $B \to X_S + \gamma$, *Z. Phys.* C **60**, 433 (1993).

[25] P. Ball, The Decay $B \to K^*\gamma$ from QCD Sum Rules, TUM-T31-43/93.

[26] A. Ali, V.M. Braun, and H. Simma, Exclusive Radiative B Decays in the Light-Cone QCD Sum Rule Approach, *Z. Phys.* C **63**, 437 (1994).

[27] C. Bernard, P. Hsieh, and A. Soni, $B \to K^* + \gamma$ and $B_s \to \phi + \gamma$ on the Lattice, *Phys. Rev. Lett.* **72**, 1402 (1994).

[28] B. Holdom and M. Sutherland, Simply Modeling $\bar{B} \to \bar{K}^*\gamma$, *Phys. Rev.* D **49**, 2356 (1994).

[29] S. Narison, $B \to K^*\gamma$ from hybrid sum rule, *Phys. Lett.* B **327**, 354 (1994).

[30] K.C. Bowler *et al.*, Probing with Penguins: A Lattice Calculation of the Branching Ratio for Some of the Exclusive Modes of $b \to s\gamma$, Edinburgh-94-544 (1994).

[31] M. Ciuchini *et al.*, $b \to s\gamma$ and $b \to sg$: A Theoretical Reappraisal, *Phys. Lett.* B **51**, 137 (1994).

[32] J. Tang *et al.*, Hadronic Matrix Elements and Radiative $B \to K^*\gamma$ Decay, *Phys. Rev.* D **51**, 3501 (1995).

[33] J. M. Soares, Constraints on V_{td} from radiative decays of the B meson, *Phys. Rev.* D **49**, 283 (1994).

[34] C.Greub, H. Simma, and D. Wyler, Branching ratio and direct CP-violating rate asymmetry of the rare decays $B \to K^*\gamma$ and $B \to \rho\gamma$, *Nucl. Phys.* B **434**, 39 (1995).